Special issue research article

NMR IN BIOMEDICINE

Received: 1 December 2014, Revised: 29 June 2015, Accepted: 17 July 2015, Published online in Wiley Online Library: 15 September 2015

(wileyonlinelibrary.com) DOI: 10.1002/nbm.3376

Residual quadrupole interaction in brain and its effect on quantitative sodium imaging

Robert W. Stobbe* and Christian Beaulieu

Sodium MRI is particularly interesting given the key role that sodium ions play in cellular metabolism. To measure concentration, images must be free from contrast unrelated to sodium density. However, spin 3/2 NMR is complicated by more than rapid biexponential signal decay. Residual quadrupole interactions (described by frequency $\overline{\omega}_Q$) can reduce M_{xy} development during RF excitation. Three experiments, each performed on the same four healthy volunteers, demonstrate that residual quadrupole interactions are of concern in quantitative sodium imaging of the brain. The first experiment shows a reliable increase in the rate of excitation 'flipping' (1%–6%), particularly in white matter with tracts running superior–inferior (i.e. parallel to B_0). Increased flip-rates imply an associated signal loss and are to be expected when $\overline{\omega}_Q \sim \omega_1$. The second experiment shows that a prescribed flip-angle decrease from 90° to 20°, with concomitant decrease in T_E from 0.25 ms to 0.10 ms and no T_1 weighting, results in a 14%–26% saline calibration phantom normalized signal (S_N) increase in the white matter regions. The third experiment shows that this (S_N) increase is primarily due to a residual quadrupole effect, with a small contribution from T_2 weighting. There is an observed deviation from the spin 3/2 biexponential curve, also suggesting $\overline{\omega}_Q$ dephasing. Using simulation to explain the results of all three experiments, a model of brain tissue is hypothesized. It includes one pool (50%) with $\overline{\omega}_Q = 0$, and another (50%) in which $\overline{\omega}_Q$ has a Gaussian distribution with a standard deviation of 625 Hz. Given the result of the second experiment, it is suggested that the use of reduced flip-angles with large ω_1 will provide more accurate measures of sodium concentration than 'standard' methods using 90°pulses. Alternatively, further study of sodium $\overline{\omega}_Q$ may provide a means to explore tissue structure and organization. Copyright © 2015 John Wiley & Sons, Ltd.

Keywords: sodium; MRI; quantitative; quadrupole; human; brain; white matter

INTRODUCTION

Sodium (^{23}Na) MRI of the brain is growing in interest with a rapidly increasing number of high field scanners with multinuclear capability. The primary and driving hope is that sodium concentration correlations with pathology will provide new insights into disease mechanisms and facilitate improved diagnosis and prediction of disease progression. Recent sodium MRI studies of the brain include multiple sclerosis (1–3), Alzheimer's disease (4), Huntington's disease (5), cancer (6,7) and stroke (8,9).

To accurately measure sodium concentration in the human brain with MRI, the acquired signal must be free from NMR contrast unrelated to sodium concentration. Minimization of relaxation weighting with short echo time (T_E) sequences has been of primary concern for more than 20 years, as the sodium nuclei in brain tissue exhibit rapid biexponential T_2 relaxation with a measured fast component (60%) as short as 1.7 ms (10). However, spin 3/2 NMR is complicated by more than rapid relaxation. ^{23}Na spin dynamics are dominated by environmental electric field gradient (EFG) induced orientation of the nuclear electric quadrupole moment with respect to the B_0 field (11). If this quadrupole interaction is static (as in a crystal), it will split the ^{23}Na resonance into three frequencies: a central resonance (40%) and two satellites (30%), each spaced from the central resonance by the interaction frequency ω_Q. However, in biological systems ω_Q will fluctuate with time as the sodium ions tumble through their environment. This dependence is given in Equation [1], where eQ is the electric quadrupole moment of the nucleus, eq is the principal EFG value and θ is the polar angle describing the orientation of eq with respect to the main magnetic field (11).

$$\omega_Q(t) = \frac{eQ\,eq(t)}{4\hbar}\left(3\cos^2\theta(t) - 1\right). \quad [1]$$

For quantitative sodium concentration imaging thus far, it has effectively been assumed that the EFGs experienced by the

* *Correspondence to: R. W. Stobbe, Department of Biomedical Engineering, Faculty of Medicine and Dentistry, University of Alberta, Edmonton, Alberta, Canada.*
E-mail: rstobbe@ualberta.ca

R. W. Stobbe, C. Beaulieu
Department of Biomedical Engineering, Faculty of Medicine and Dentistry, University of Alberta, Edmonton, Alberta, Canada

Abbreviations used:: *α, prescribed flip-angle; ASC, apparent sodium concentration; EFG, electric field gradient; eQ, electric quadrupole moment of nucleus; eq, principal EFG value; BS, brain stem; CB, cerebellum; CC, corpus callosum; CSF, cerebral spinal fluid; CSV, centrum semiovale; DQMA, double-quantum magic angle; IC, internal capsule; M_{xy}, transverse magnetic moment; PSF, point spread function; φ, resultant flip-angle; R_f, relative flip-rate; ROI, region of interest; S_N, saline calibration phantom normalized signal; SNR, signal to noise ratio; θ, polar angle describing the orientation of eq with respect to B_0; ω_Q, (time dependent) quadrupole interaction frequency;* $\overline{\omega}_Q$, residual (time averaged) quadrupole interaction frequency.

tumbling ^{23}Na nuclei are isotopically distributed in 3D space, and that this tumbling (and the resultant fluctuation of ω_Q) is sufficiently rapid to yield a time-averaged (or residual) $\overline{\omega}_Q = 0$. This is indeed the case in saline water, where isotropic EFGs result from very rapid fluctuations of the hydration shell (with correlation times much smaller than the Larmor period). In this case there is no residual quadrupole interaction or splitting of the ^{23}Na resonance. However, in biological environments the presence of charged macromolecules (12) and lipid membranes (13) may result in additional superimposed EFGs. A residual quadrupole interaction will be produced if the correlation times of the resultant EFGs experienced by the tumbling nuclei become greater than ω_Q^{rms} (11). It has been demonstrated with double-quantum magic-angle (DQMA) spectroscopy and imaging that at least some sodium nuclei within the human brain exist in environments that produce residual quadrupole interactions (14,15).

When the magnitude of $\overline{\omega}_Q$ approaches $\omega_1 = \gamma B_1$, irrecoverable signal loss begins to occur (16). This phenomenon would influence the measurement of absolute sodium concentration (in mM) in the brain with MRI. However, we are aware of only one published sodium MRI paper that considered this effect, a 1987 study that found no evidence of detrimental residual quadrupole interaction in excised cat brain (17). To search for residual quadrupole interactions with $\overline{\omega}_Q$ approaching ω_1 (and thus the presence of signal loss), this former study searched for a second intriguing consequence of these large interactions, that is, an increase in rate of magnetic moment flipping during the RF pulse (16). If the RF bandwidth is sufficiently narrow with respect to $\overline{\omega}_Q$, only the central component of the split ^{23}Na spectrum will be excited. 'In this case the magnetization behavior is approximately like that of a single "fictitious" spin ½ particle (18). This fictitious particle, however, responds to the applied RF field with an effective gyromagnetic ratio that is larger than that of the sodium nucleus as a whole' (quote from Reference 17). Interested readers are pointed to Reference 16 for an equation underlying this process. For very large $\overline{\omega}_Q$ the effective flip-rate is twice that prescribed (i.e. prescribing ω_1 for a 90° RF pulse yields a 180° flip), and the maximum transverse magnetic moment achievable is only 0.2 M_0.

The ultimate purpose of this paper is to determine whether residual quadrupole interactions with $\overline{\omega}_Q$ values great enough to affect the quantification of sodium concentration with standard MRI methods exist in human brain. This work includes three experiments, which together identify a phenomenon that must be considered when generating quantitative sodium concentration maps of the human brain.

MATERIALS AND METHODS

General image acquisition

Sodium imaging was done on a 4.7 T Varian Inova scanner using an in-house designed and constructed single-tuned sodium birdcage coil. *k*-space was sampled with twisted projection imaging designed to produce a $\beta = 3$ Kaiser filtering shape with sampling density (19). In each experiment a trajectory set consisting of 2400 trajectories sampled *k*-space to a spheroid with maximum dimensions of 118 1/m × 118 1/m × 59 1/m (unless otherwise specified). In each case the readout duration was 15 ms. For each image the RF excitation pulse was non-selective and the delay between the end of the RF pulse and the acquisition of the centre of *k*-space was 0.05 ms. The image reconstruction process involved sampling density compensation to achieve the filtering shape throughout *k*-space (i.e. compensation at the centre of *k*-space before initiation of twisting) and standard 3D gridding.

For each of Experiments 1–3 described below, the same four healthy volunteers with ages 27, 38, 27 and 23 years were scanned. Each experiment was less than 45 min in duration and was conducted in a separate imaging session. For Experiments 1 and 2, volunteers were scanned with calibration tubes on either side of their heads. The tubes were about 3 cm in diameter, about 11 cm in length and contained 50 mM saline water. All of the acquired images were co-registered (in-house software) and the same regions of interest (ROIs; identified below) were used between experiments.

In the experiments described below and throughout the remaining text, the prescribed flip-angle ($\alpha = \omega_1 t$) is the flip-angle setting of the spectrometer following RF power calibration. However, the prescribed flip-angle (α) is not necessarily attained. Here we introduce a term called the relative flip-rate (or R_f) where φ is the resultant flip-angle produced (Equation [2]). In the context of residual quadrupole interactions, the value of R_f is 1 in regions where $\overline{\omega}_Q = 0$, and greater than 1 (to a maximum of 2) when $\overline{\omega}_Q \geq \omega_1$. Note that the specific theoretical dependence of R_f on $\overline{\omega}_Q$ and ω_1 can obtained in Reference 16.

$$\phi = R_f \omega_1 t \qquad [2]$$

Experiment 1. Constant-T_E flip-angle experiment

This experiment consisted of the generation of two 10 min images, one with a prescribed flip-angle of α = 60° and the other a prescribed flip-angle of α = 120°. A relative flip-rate (R_f) map was obtained from these two images (Equation [4]). Note that $S_{(\alpha = 60°)}$ and $S_{(\alpha = 120°)}$ are the signal intensities in the respective α = 60° and α = 120° flip-angle images. With a little trigonometry Equation [4] can be derived from Equation [3].

$$\frac{S_{(\alpha=60°)}}{S_{(\alpha=120°)}} = \frac{\sin(R_f \alpha)}{\sin(R_f 2\alpha)} \qquad [3]$$

$$R_f = \cos^{-1}\left(1/\left(2S_{(\alpha=60°)}/S_{(\alpha=120°)}\right)\right)/60° \qquad [4]$$

Low spatial frequency variation in the R_f map was assumed to be the result of coil-related B_1 variation (20,21). This low-frequency variation was assessed with low-pass filtering and removed. The same RF pulse length (τ_{RF}) of 0.5 ms and T_E of 0.285 ms were used for both flip-angle images to avoid any dependence on T_2, and both images were generated with a long T_R of 250 ms to avoid T_1 weighting (T_1 in cerebral spinal fluid (CSF) is 65 ms at 4.7 T). R_f maps were generated from each of the healthy volunteers, and average values were measured in different ROIs manually placed on axial slices. These included the saline calibration phantoms and the CSF, ^{23}Na environments that should not exhibit residual quadrupole effects. Other ROIs included regions with visible R_f increase on each map: centrum semiovale (CSV), internal capsule (IC), brain stem (BS), and corpus callosum (CC), genu and splenium combined. The analysis of cortical gray matter is difficult on these low resolution images,

as it is not easily separated from CSF. For this reason it was excluded from analysis. However, an ROI of the cerebellum (CB) was included, as this structure was easily isolated.

Experiment 2. Constant- ω_1 flip-angle experiment

For a prescribed flip-angle of $\alpha = 90°$, $R_f > 1$ will produce an actual flip-angle $\phi > 90°$ and exacerbate signal loss for nuclei experiencing residual quadrupole interactions. For prescribed flip-angles $\alpha < 90°$, $R_f > 1$ will produce actual flip-angles closer to 90° than prescribed, thus mitigating residual quadrupole related signal loss. If significant residual quadrupole interactions are present in a given tissue the *relative* signal from that tissue, with respect to signal from the saline calibration phantoms (or the saline calibration phantom normalized signal – S_N) is expected to increase when the prescribed flip-angle is reduced. Note that a constant S_N is expected for all prescribed flip-angles in tissue regions that did not exhibit elevated R_f in Experiment 1 (i.e. CSF) – this was also tested. Calibration phantom normalization is typically used to provide sodium concentration maps and quote concentration values, and an S_N increase would reflect a 'concentration' increase. Here we refrain from attaching concentration numbers to S_N, as these numbers are influenced by residual quadrupole interaction and RF excitation (as well as rapid T_2 decay and partial volume effects).

In Experiment 1 the $\alpha = 120°$ image was created with $\omega_1 = 667$ Hz, while the $\alpha = 60°$ image had $\omega_1 = 333$ Hz. This was done to maintain a constant τ_{RF} and T_E, thus avoiding contrast dependence on T_E. However, the reduction of ω_1 for the $\alpha = 60°$ pulse will increase residual quadrupole related signal loss during that pulse and reduce the measureable R_f effect. In Experiment 2, four images were acquired with $\alpha = 90°$, 60°, 40°, and 20°, each applied with constant $\omega_1 = 625$ Hz. This involved τ_{RF} reduction (0.40 ms, 0.27 ms, 0.18 ms, and 0.09 ms), which was also used to reduce T_E (0.252 ms, 0.87 ms, 0.142 ms, and 0.097 ms). T_R was also reduced to 210 ms (90°), 170 ms (60°), 130 ms (40°), and 70 ms (20°) to shorten the scan durations while maintaining a consistently small (2%) T_1 weighting in saline. Note that for the $\alpha = 20°$ scan three averages were acquired to increase signal to noise ratio (SNR). A B_1 map was also acquired using a two flip-angle approach. However, to produce a map of just low spatial frequency variation a trajectory set with only 440 trajectories was used, sampling *k*-space to 50 1/m × 50 1/m × 50 1/m in 1.8 min (with one average). Following B_1 correction, image signal was measured in the saline calibration phantoms and the ROIs described above in Experiment 1. For each region and for each volunteer the saline calibration phantom normalized sodium signal (S_N) measured in the $\alpha = 60°$, 40°, and 20° images was plotted in proportion to the S_N from the $\alpha = 90°$ image.

Experiment 3. Signal decay variation from biexponential

There were two purposes of this experiment. First, in the presence of residual quadrupole interactions, oscillation and/or dephasing of the satellite signal (i.e. the signal produced from outer spin 3/2 quantum transitions) should impact the measured signal decay after excitation. In this case dephasing results from differing $\overline{\omega}_Q$ values experienced by nuclei within different tissue 'domains' (22) inside the voxel. Thus, the first purpose of this experiment was to search for signal decay deviation from a biexponential shape. The second purpose of this experiment was to determine whether signal decay alone could explain the relative signal increase with reduced flip-angle prescription (and shorter T_E) in Experiment 2. T_E values of 0.143 ms, 0.266 ms, 0.616 ms, 1.02 ms, 2.02 ms, 3.02 ms, 4.02 ms, 10 ms, and 20 ms were used to develop the signal decay curves. For this experiment $\alpha = 40°$ with $\tau_{RF} = 0.18$ ms and T_R was set to 75 ms. A reduced α with short τ_{RF} was used to attain a short T_E of 0.143 ms for the first image. Each of the nine images took 3 min to acquire. The scope of this analysis was limited to the IC region of the brain, a region showing both $R_f > 1$ in Experiment 1 and S_N increase with reduced α in Experiment 2. This region is also easily isolated from CSF contamination and is sufficiently large to allow high confidence measures of mean signal (with respect to image noise (23)). If a large residual quadrupole effect is present in tissue with an $\overline{\omega}_Q$ sufficient to produce $R_f > 1$, initial T_E values (those less than 1 ms) should be altered from simple spin 3/2 biexponential relaxation. For this reason the fast (60%) and slow (40%) relaxation components were fitted to the remaining six data points from 1 ms to 20 ms (least-squares regression). The curves were then plotted to determine whether they would also describe the signal decay at the time points < 1 ms. To ensure the reliability of this experiment, a 5% agar (50 mM sodium) phantom was scanned with this same protocol. Residual quadrupole interactions are not expected in agar phantoms, and the measured signal decay should be strictly biexponential. Finally, initial signal decay was assessed by fitting a single exponential to the first three data points ($T_E < 1$ ms). This time constant was used to assess the impact of signal decay alone on the signal increase measured in Experiment 2.

RESULTS

Experiment 1

Regions of brain tissue that generate residual quadrupole interactions of sufficient $\overline{\omega}_Q$ are expected to flip at a greater rate than environments without any effect such as CSF and saline. A representative R_f map from one of the healthy volunteers is shown in Figure 1. Tissues in which one might expect long range macromolecular order such as white matter show statistically ($p \leq 0.01$) elevated R_f (1.01–1.06) with respect to CSF (~0.99) and saline (~0.99) (Fig. 2). However, the CB is not significantly different from CSF. Brain regions with white matter tracts running superior–inferior (i.e. parallel to the static field B_0) demonstrate greater R_f. Both the BS (1.06) and IC (1.04) show statistically elevated ($p \leq 0.02$) R_f with respect to the CC (1.01), which has tracts running perpendicular to B_0. Note that a paired *t* test was used to test for significance at $p < 0.05$.

Experiment 2

Figure 3 depicts the saline calibration phantom normalized signal (S_N) increase in brain tissue when the prescribed flip-angle is decreased from $\alpha = 90°$ to $\alpha = 20°$ (along with T_E reduction from 0.252 to 0.097 ms). This increase is apparent in the CSV (green arrows), the posterior limb of the IC (red arrows), and the BS (blue arrows). Another very obvious increase is visible in the skin. For each volunteer, and particularly in white matter regions, prescribed flip-angle reduction ($\alpha = 60°$, 40°, 20°) monotonically increases S_N relative to the $\alpha = 90°$ image (Figure 4). On average these increases are (7%, 11%, 14%) for CSV, (10%, 14%, 18%) for IC, (11%, 16%, 26%) for BS, and (7%, 12%,

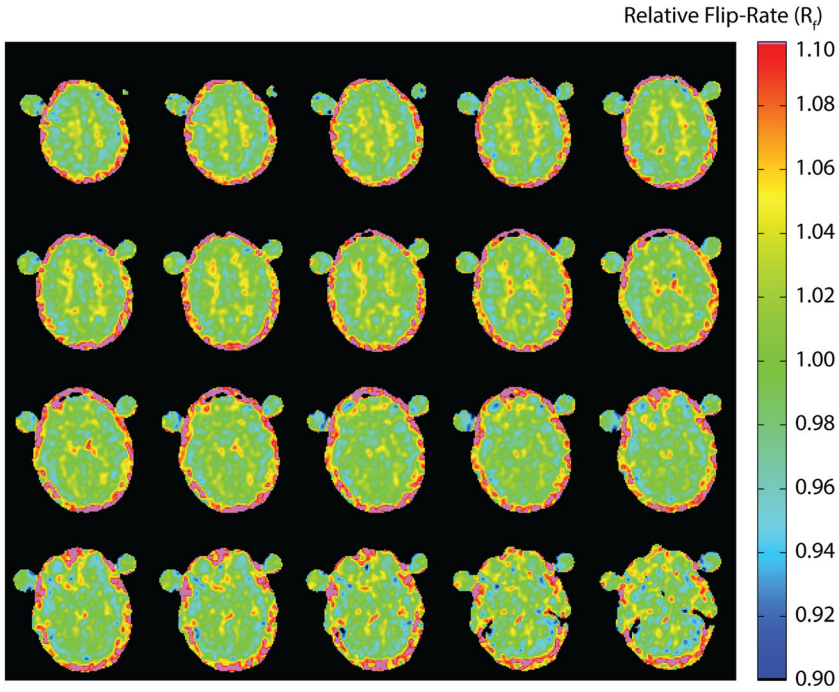

Figure 1. A representative relative flip-rate (R_f) map from Volunteer #3. White matter regions throughout the brain, as well as the brain stem show elevated R_f with respect to CSF, the two anterior saline calibration phantoms, and surrounding tissue. The skin in particular also demonstrates elevated R_f.

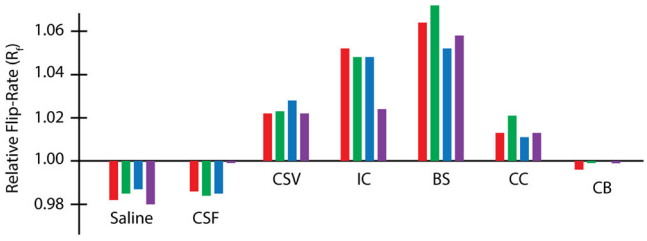

Figure 2. Relative flip-rates (R_f) from all 4 volunteers (each represented by a different colour). As is visible in the Volunteer #3 image of Figure 1 (blue bar in this graph), white matter regions produce reliably greater R_f than either CSF or the saline calibration phantoms. In particular, regions with tracts running superior-inferior parallel to B_o, i.e. centrum semiovale (CSV), posterior limb of internal capsule (IC) and brain-stem (BS), yield the greatest Rf; rates greater than the left-right corpus callosum (CC). The cerebellum (CB), with less white matter and tracts primarily perpendicular to B_o, does not exhibit a change in relative flip-rate.

14%) for CC. This is in contrast to S_N from CSF, which remains essentially constant (1%, 2%, 3%) with reduced α. The CB shows a small average increase of (4%, 6%, 9%).

Experiment 3

The first part of this experiment involved investigation of deviation from biexponential decay, as a separate means of detecting residual quadrupole interactions. Agar is not expected to produce a residual quadrupole interaction, and a spin 3/2 biexponential signal decay curve fits the T_2* relaxometry data very well, with $T_{2fast} = 2.05$ ms and $T_{2slow} = 16.1$ ms (Fig. 5(a), (b)). However, this biexponential curve does not fit the brain tissue volunteer data nearly as well, as seen for the IC in Figure 5(c), (d). There seems to be a more rapid initial decay in the brain data. If the first three data points are excluded from the least-squares fitting, the regressed biexponential curve still bisects those first three points for the agar environment (Fig. 5(a), (b)). However, this is not the case for the IC ROI data from the healthy volunteer (Fig. 5(c), (d)). In fact, for each volunteer the initial data measured from the IC is above the biexponential regression that fits the remainder of the data points (Fig. 6).

The second part of this experiment involved an investigation of whether the T_2 relaxation was sufficient in itself to explain the results of Experiment 2. In Figure 6 a single exponential is fit through the first three data points to provide an indication of the rate of initial signal decay (in the region of the IC). For the most rapid initial decay measured (3.3 ms from Volunteer 2), this decay would result in a 5% signal increase when T_E is reduced from 0.252 ms to 0.097 ms, as it is in Experiment 2. However, Figure 4(b) shows about 20% increase in signal (relative to the saline calibration phantoms) for Volunteer 2 when α is reduced from 90° to 20° (and T_E reduced from 0.252 ms to 0.097 ms). Thus, the reduction of T_2-relaxation related signal loss with shorter T_E values is not sufficient to describe the results of Experiment 2. This supports the reduction of residual quadrupolar related signal loss as a mechanism of S_N increase when α is reduced from 90° to 20°.

DISCUSSION

Particularly in white matter regions of the brain with tracts running superior–inferior (or parallel to B_0), the constant-T_E flip-angle experiment (Figs. 1 and 2) and the constant- ω_1 flip-angle experiment (Figs. 3 and 4) point to the presence of residual quadrupole interactions. Note that an orientation dependence is not surprising given the residual quadrupole $\overline{\omega}_Q \propto 3\cos^2(\theta) - 1$ relationship with the B_0 field. In spin 3/2 ^{23}Na environments

NMR IN BIOMEDICINE

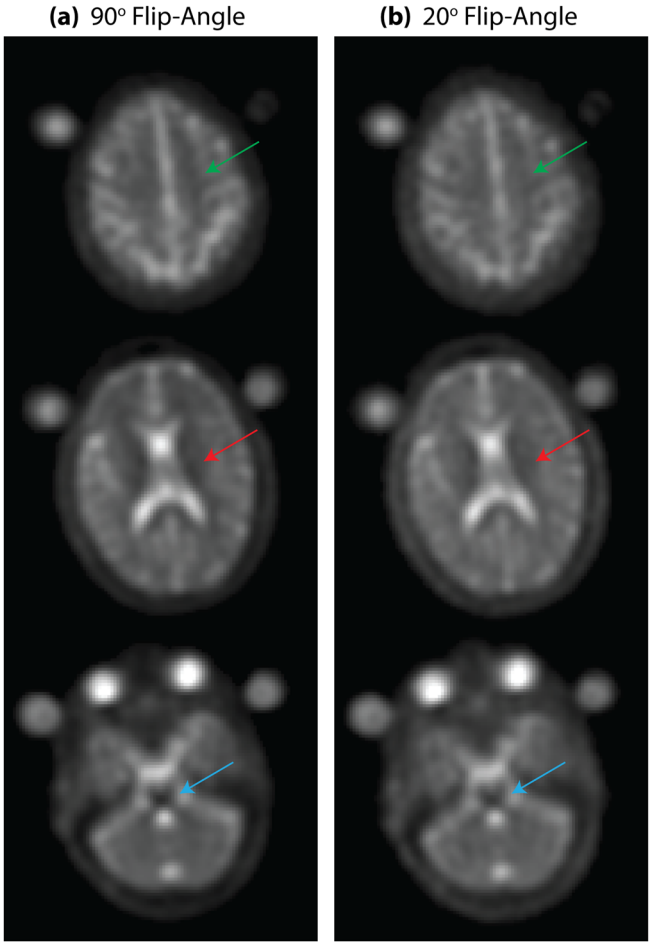

Figure 3. The relative sodium signal in primarily white matter (with respect to that from the saline calibration phantoms) increases as the prescribed flip-angle is reduced from $\alpha = 90°$ (**a**) to $\alpha = 20°$ (**b**). Note that image intensity for both the $\alpha = 90°$ and $\alpha = 20°$ images has been normalized according to signal from the saline calibration phantoms. Regions highlighted in this image from Volunteer #3 include the centrum semiovale (top-green arrows), posterior limb of the internal capsule (middle - red arrows) and brain stem (bottom - blue arrows). Calibration phantom normalized signal (S_N) increase in the skin is also clearly visible on the 20° image. This is in contrast to the CSF and eyes (vitreous humour) that show little difference between the two sets of images.

where $\overline{\omega}_Q$ is in the range of ω_1, the nuclear ensemble will flip at a faster rate than otherwise prescribed by the RF pulse. The result of increased flip-rate (R_f) in white matter regions of the brain (Experiment 1) cannot be explained by a T_2 effect (a constant T_E was used). In the constant- ω_1 experiment (Experiment 2), the saline calibration phantom normalized signal (S_N) in white matter regions of the brain increased by about 5% to about 25% as the prescribed flip-angle was reduced from $\alpha = 90°$ to $\alpha = 20°$. As Experiment 3 demonstrates, these S_N increases cannot be explained by the concomitant T_E reduction in Experiment 2. This supports the theory that prescribed flip-angle reduction mitigates residual quadrupole signal loss in white matter regions of the brain. Because residual quadrupole interactions produce irrecoverable signal loss during the RF excitation pulse, the magnitude and consequence of this effect must be assessed for the quantitative measurement of sodium concentration in the brain.

The T_2* relaxometry curves of Figure 6 provide an initial hint regarding the sodium environment in the brain, and here we turn to simulation to help develop some understanding. Note that the simulation was performed by solving the sets of differential equations that describe the evolution of the spin 3/2 nuclear ensemble (24). The value of ω_1 in Experiment 3 was 625 Hz. If one assumed that all sodium nuclei experienced an $\overline{\omega}_Q$ of 625 Hz together with a T_{2fast} of about 4 ms and a T_{2slow} of about 35 ms (from Fig. 6), the signal decay curve would look like the solid line in Figure 7. Note that an ideal (extremely short) RF excitation is used for this simulation. Oscillation in Figure 7 is associated with the 'outer transitions' between the four (shifted in this case) sodium energy-states. These are the transitions that give rise to 60% of the signal as well as the fast component of T_2 relaxation. Note that this oscillation would produce the two expected satellite peaks if one were to take the Fourier transform. However, no large oscillation is observed in Figure 6. Therefore, if large $\overline{\omega}_Q$ values do exist in the brain, we must assume that they take on some distribution from one 'domain' to another. For a Gaussian distribution (25) with zero mean and an $\overline{\omega}_Q$ standard deviation of 625 Hz, the signal decay looks like the dotted line in Figure 7. In this case the oscillation disappears and is replaced with a rapid decay to 40% of the signal associated with T_{2slow}. The signal decay shape of the dotted line is not observed in Figure 6 either. However, Figure 6 does suggest a rapid initial decay that deviates from the overall biexponential shape. Thus, we suggest that brain tissue exhibiting $R_f > 1$ (e.g. white matter) may be composed of two 'pools' of sodium nuclei. A simple theoretical model includes one pool exhibiting biexponential signal decay with $\overline{\omega}_Q = 0$ Hz (perhaps intracellular sodium), and the other a Gaussian distribution of $\overline{\omega}_Q$ (perhaps interstitial sodium within the wraps of myelin). Together, the signal from these pools could produce the shape in Figure 6. Note that the rate of initial decay for the Gaussian distribution pool is dependent on the standard deviation of $\overline{\omega}_Q$. For a standard deviation of 625 Hz the initial rapid decay ends at approximately the same time as observed in Figure 6. For this reason it was chosen as a potential model for brain tissue. Before estimating a distribution of these two pools we turn to simulation of Experiments 1 and 2 to determine whether an $\overline{\omega}_Q$ standard deviation of 625 Hz could explain these results as well.

The evolution of the transverse magnetic moment of Experiment 1 is shown in Figure 8 for an $\overline{\omega}_Q$ standard deviation of 625 Hz. Note that the prescribed $\alpha = 60°$ and $\alpha = 120°$ RF pulses should both produce the same M_{xy} value (of 0.87 M_0) (red trace). However, the 60° RF pulse produces a greater M_{xy} than the 120° RF pulse, while both produce values lower than 0.87 M_0 (black trace). As the signal decays following the RF pulse, the relative M_{xy} difference increases between the $\alpha = 60°$ and $\alpha = 120°$ curves. The signal from the outer transitions has been dephased at about 1 ms. The signal difference at this point arises from an increased rate of flipping (R_f) 'expressed' in the slow decaying M_{xy} component. For this simulation an R_f increase of 18% can be calculated from the relative values at 1 ms. If the values at T_E are used, the calculated R_f increase will be 7%. If one assumes that this residual quadrupole interaction pool accounts for about 50% of the total sodium concentration, the calculated R_f increase will be 3% at T_E and 5% at 1 ms, values similar to those measured in Experiment 1 (Fig. 2). Note that off-resonance will also alter the rate of flipping (in this case $R_f = \omega_{eff}/\omega_1$ in Equation [2]). However, to produce the approximately 5% difference in R_f between white matter and the directly adjacent CSF, the CSF would need to be more than 250 Hz off resonance (with the adjacent white matter on resonance). We have shown the majority of brain tissue to be within ± 10 Hz at 4.7 T (aided by a gyromagnetic ratio about one-quarter that of ^{1}H) (26).

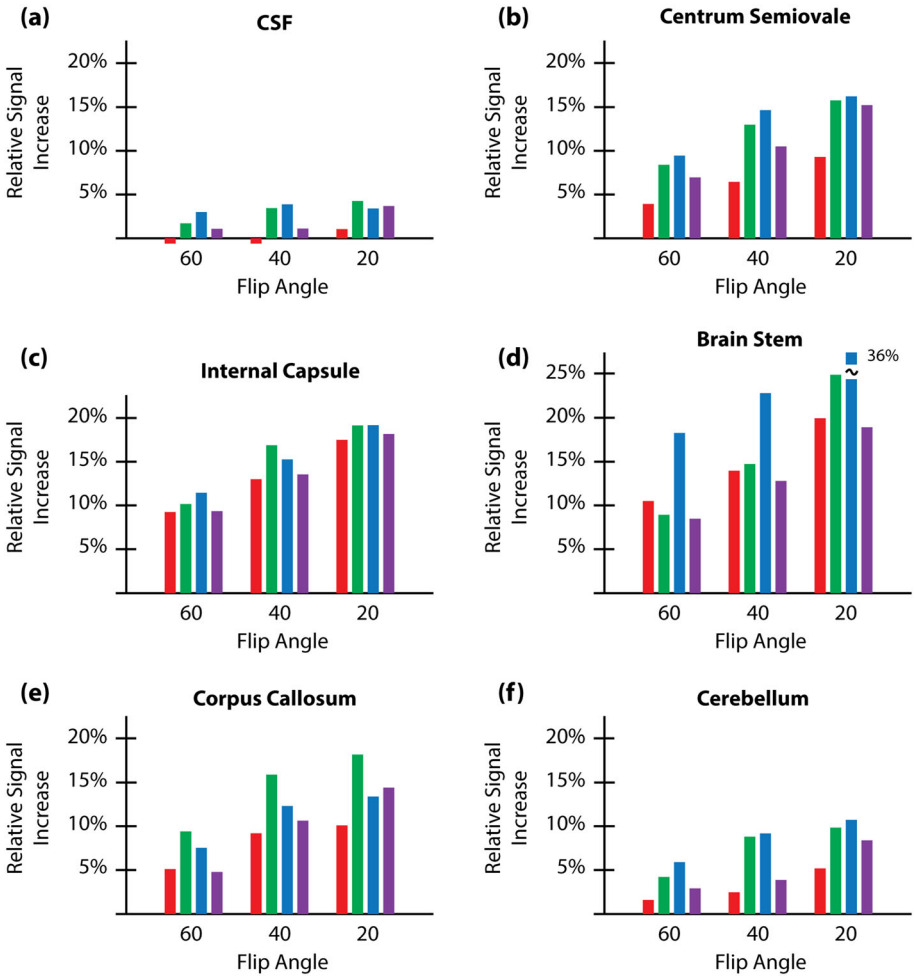

Figure 4. Saline calibration phantom normalized ^{23}Na signal (S_N) is substantially and monotonically increased with flip-angle reduction (from $\alpha = 90°$), particularly in the (c) internal capsule and (d) brain stem. In comparison, the S_N from (a) CSF remains stable with flip-angle reduction.

As the prescribed flip-angle is reduced from α = 90°, the increased rate of flipping helps mitigate inherent signal loss associated with the residual quadrupole interaction. Consider the extreme case when $\overline{\omega}_Q \gg \omega_1$. In this case only 'inner-transition' signal will be produced by the RF pulse in an amount defined by $M_{xy} = 0.2 \sin(2\alpha) M_0$ (16). If α = 90° is used, no signal will be produced from these nuclei. However, for small α the relative M_{xy} generated will be about $0.4 \sin(\alpha) M_0$. This is approximately the maximum relative signal that can be contributed by the inner transition. Simulations of the RF excitation pulses of Experiment 2 are shown in Figure 9 for an environment in which $\overline{\omega}_Q$ has a standard deviation of 625 Hz. In this case M_{xy} is plotted relative to the signal that should be produced from a $\sin(\alpha)$ RF pulse. The relative contributions from both the inner and outer transitions are increased with reductions in α. If the residual quadrupole pool accounts for 50% of the sodium nuclei, the expected sodium measurement increase from the 90° case would be 8% (60°), 12% (40°), and 17% (20°) – taking into account the values at T_E (indicated by a cross in Fig. 9). These increases are similar to the measured values given in Figure 4.

Considering simulation of Experiments 1 and 2, a brain tissue model in which 50% of the ^{23}Na nuclei experience a Gaussian distribution of $\overline{\omega}_Q$ (with standard deviation of 625 Hz) fits the measured data quite well. However, it should be noted this model remains a hypothesis, and further study may refine or alter this model. Returning to discussion of signal decay, we note from Figure 7 that the outer-transition signal produced in an environment with an $\overline{\omega}_Q$ standard deviation of 625 Hz has completely dephased by 1 ms (at a rate that could be described by an exponential with ~0.25 ms time constant). Thus, the fast : slow T_2* ratio beyond 1 ms for the proposed model should be 43% fast and 57% slow (assuming both pools have the same slow component of relaxation). Fitting this model to the data of Experiment 3 yields T_{2fast} values in the $\overline{\omega}_Q$ = 0 Hz pool of 2.4 ms, 2.5 ms, 2.3 ms, and 2.4 ms for volunteers 1–4, respectively; similarly, the fitted T_{2slow} values for both pools are 21 ms, 18 ms, 18 ms, and 19 ms. Note that the *r*-squared values are essentially the same for both fitting methods: an average of 0.9994 for Figure 6 and an average of 0.9997 for the proposed model. Simulation of signal decay for the proposed model is given in Figure 10. Note that this simulation does not match the data in Figure 6, as the signal in the initial rapid decay is much greater than in Figure 6. However, there is an explanation. The first data point with $T_E = 0.143$ ms will contain very rapid signal decay around the centre of *k*-space such that the signal associated with this rapid decay will be widely spread (at a greatly reduced value) throughout the image. Thus, the signal associated with the initial data points is probably much greater than that measured in Experiment 3. On the other hand, the $T_E > 1$ ms data points will not be affected by extreme central *k*-space signal

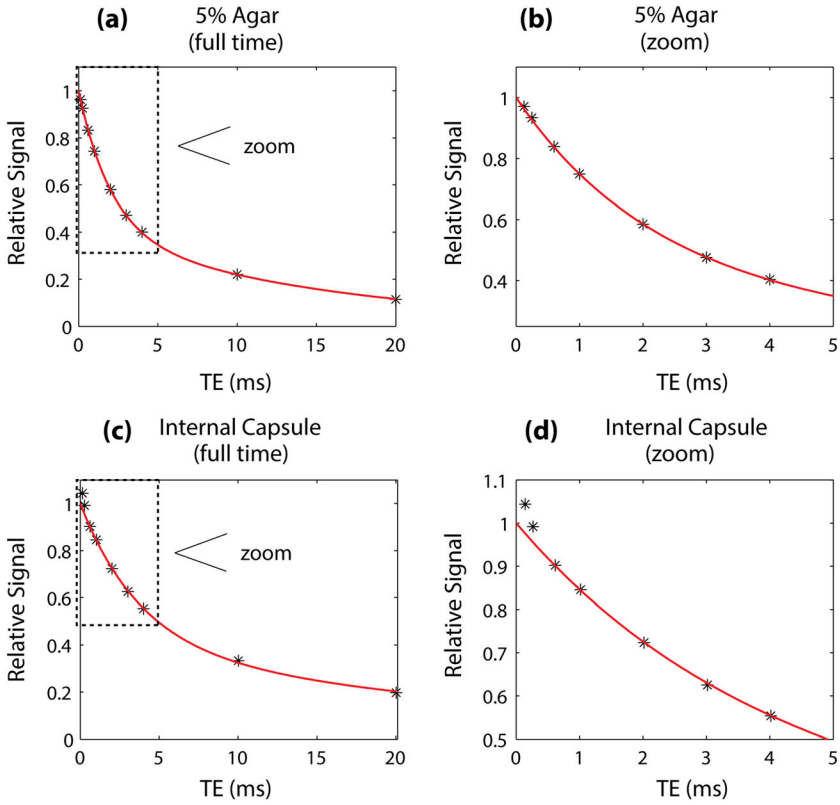

Figure 5. Signal decay as a function of TE measured from 5% agar (**a and b**) as well as from the internal capsule of Volunteer #2 (**c and d**). The spin 3/2 biexponential curve fits the measured data from the agar phantom extremely well. However, the initial 2 data points from the volunteer data (measured in the internal capsule area) are elevated above the biexponential curve that fits the remainder of the data points. These two data points suggest a more rapid initial decay.

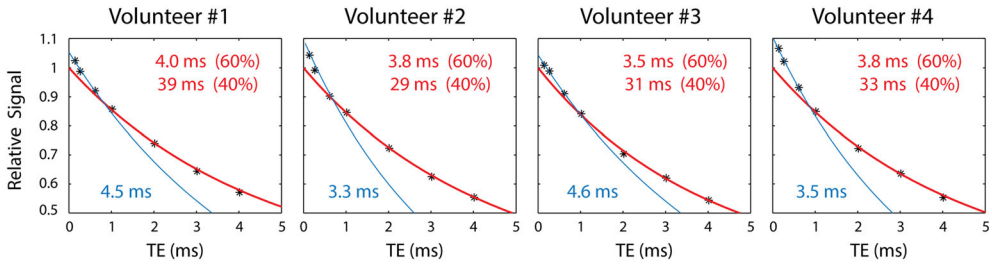

Figure 6. Signal measured from the internal capsule region shows more rapid initial decay than the spin 3/2 biexponential curve that fits the remainder of the data points (red line). The values describing each biexponential curve are given for each volunteer in red. The blue line show single exponential fitting for the first 3 data points (with the fitted value also given in blue). This curve is drawn to provide an indication of how rapidly the initial signal decays.

drop-off. Imaging techniques that facilitate localization of very rapid signal decay are required for improved signal decay analysis. Experiments 1 and 2 will also produce images in which the initial rapidly decaying signal is poorly localized. However, for each of these experiments, the point spread function (PSF) is very similar from scan to scan, and the demonstrative effects are also expressed in the slowly decaying signal component.

When radial imaging is used with an $\alpha = 90°$ pulse such that T_E is 0.25 ms, simulation suggests that in white matter the relative M_{xy} at T_E will be 83% of its actual value, and much of this signal will be poorly localized from the very rapid decay at the centre of *k*-space (from Fig. 9 – using the two pool model). Thus, it is not surprising that papers using 90° excitation pulses and radial imaging techniques show dark regions in the white matter at the centre of the brain (see the tissue sodium concentration map in Fig. 8 of Reference 27). Gradient-echo imaging employs $T_E > 1$ ms, but is typically implemented with a reduced flip-angle that would have a mitigating effect. Regardless, the measured sodium concentration may still be less than 70% of its actual value (see the short T_E image in Fig. 2 of Reference 10). The published sodium imaging technique that may best represent sodium concentration is single-point imaging (28). This technique employs very short flip-angles, and only acquires one point of *k*-space following each excitation. Thus, single point imaging is also immune to the PSF smearing associated with rapid signal decay. Although these images are inherently low

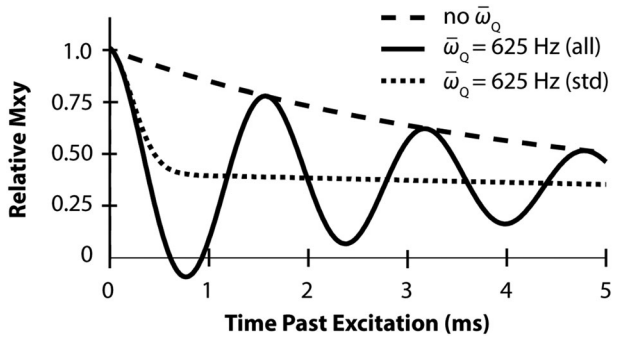

Figure 7. Simulated signal decay following an 'ideal' (or very short) RF excitation pulse. In the absence of residual quadrupole interactions the signal decay is biexponential (dashed line). If all sodium nuclei experience $\omega_Q = 625$ Hz, the signal will oscillate as shown with the solid line. However, if ω_Q is distributed in a Gaussian manner throughout the voxel with the standard deviation of ω_Q being 625 Hz, the signal will dephase as shown with the dotted line. None of the curves on its own describes the signal decay in Figure 6, however, a combination of no ω_Q (dashed) and ω_Q distributed (dotted) curves might.

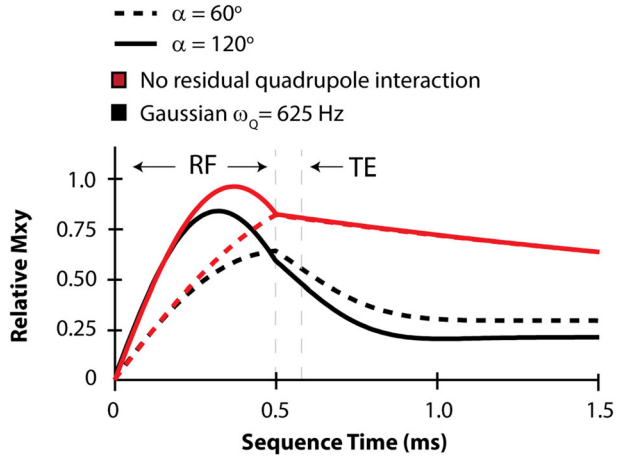

Figure 8. Simulated ^{23}Na evolution during and following excitation of the flip-rate study of Experiment #1. The prescribed $\alpha = 60°$ and $\alpha = 120°$ RF pulses should produce the same M_{xy} (red trace). However, a Gaussian ω_Q distribution of 625 Hz will increase the flip-rate (R_f) yielding larger resultant flip-angles ($\varphi = R_f\alpha$) and relatively greater signal from the $\alpha = 60°$ pulse (black trace). Note that the primary effect of a Gaussian ω_Q distribution is signal loss. Thus, the measurement of flip-rate increase in Experiment #1 points to residual quadrupole related signal loss.

resolution and have excessive scan times, they do not appear to show the same signal drop-off in the white matter at the centre of the brain. It is interesting to note that signal loss related to the outer transitions and residual quadrupole interactions is actually quite an old spectroscopy-based idea (29).

Given the localized regions of residual quadrupole interaction described in this paper, it is perhaps unexpected that a recent DQMA study did not show the same signal localization (15). The DQMA sequence selectively acquires signal from only those nuclei exhibiting residual quadrupole interaction; however, the imaging study of Reference 15 showed relatively uniform signal throughout the brain. The DQMA study acquired very low resolution images (by necessity, as this is a very low signal sequence), and the limited ability to distinguish the white matter is one possible explanation. An alternative explanation involves the RF

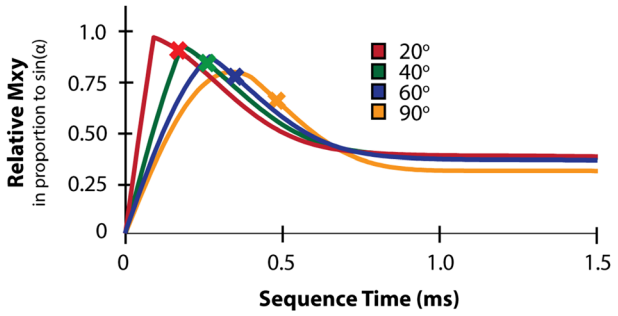

Figure 9. Simulated ^{23}Na evolution during and following excitation of the flip-angle study of Experiment #2. For this simulation the standard deviation of the Gaussian ω_Q distribution is 625 Hz. The relative signal (in proportion to what it should be (i.e. sin(α)) is increased as the prescribed flip-angle is reduced from $\alpha = 90°$ to $\alpha = 20°$. The 'x's on the figure indicate the locations at which the centre of k-space is acquired for each flip-angle.

pulse length that was used in that study. For an 'ideal' DQMA sequence with extremely short RF pulses the optimal preparation time (τ) is about 0.3 ms for a zero mean $\bar{\omega}_Q$ distribution with standard deviation of 625 Hz, and for this 'ideal' DQMA sequence the optimal $T_E = \tau$. However, the RF pulse lengths of the sequence implemented in Reference 15 were 0.5 ms long (i.e. far from the ideal case). The problem with this sequence and this study (for the $\bar{\omega}_Q$ model suggested here) is that simulation suggests that M_{xy} would have almost completely dephased by the implemented T_E for each value of τ and T_E used (the minimum was 1 ms). Thus, if local white-matter regions do contain the suggested large $\bar{\omega}_Q$ distributions, they would have produced very little signal in the DQMA sequence of Reference 15. DQMA imaging alternatives in which $T_E \neq \tau$ may improve this technique for analysis of the brain. Another approach to assess residual quadrupole interaction in the brain may include the use of a nutation filter (30). In this technique residual quadrupole derived R_f increase is *maximized* during a soft 90° preparatory pulse, and this preparatory R_f increase is used to selectively acquire signal from only those nuclei experiencing residual quadrupole interactions.

The production of a coil related B_1 map is an important part of sodium concentration measurement with MRI. However, the first experiment in this study suggests that B_1 mapping inherently includes both B_1 and residual quadrupole aspects. For this study the normalization of long range flip-rate variation was sufficient to highlight local tissue dependent regions of variation, as this localized effect could not be attributed to either T_1 (very long T_R), T_2 (constant T_E), or the coil field-map. However, when the production of an accurate B_1 map is necessary for sodium concentration measurement, care must be taken to minimize the residual quadrupole effect. Otherwise the consequence will be a B_1 over-estimation of in regions of large $\bar{\omega}_Q$, and subsequent erroneous normalization.

Sodium concentration increases have been reported for many different brain disorders. In light of the residual quadrupole effect suggested in this paper, reconsideration of these results may be warranted. While it is likely that sodium concentrations do increase with pathology, many disorders alter the macromolecular environment, e.g. multiple sclerosis, which results in demyelination. A result of demyelination may be reduction of long range order experienced by the sodium nuclei, leading to $\bar{\omega}_Q$ reduction and less signal loss. Relative to healthy controls

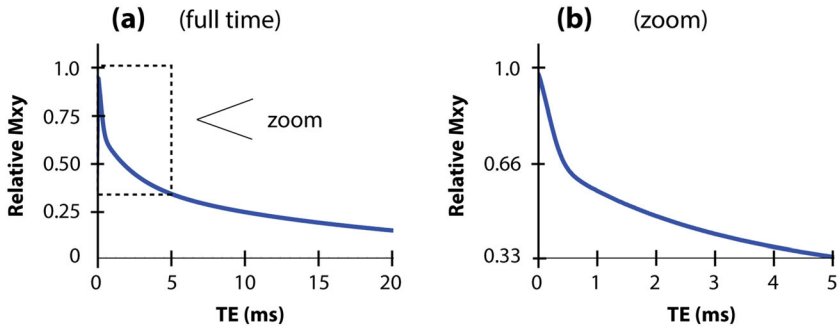

Figure 10. Simulated ^{23}Na signal decay for a model in which 50% of the nuclei experience a residual quadrupole interaction with an ω_Q standard deviation of 625 Hz, and the other 50% do not experience a residual quadrupole interaction. Relaxation values of $T_{2fast} = 2.4$ ms and $T_{2slow} = 20$ ms were used for both environments.

the result of $\overline{\omega}_Q$ reduction would be a signal increase. Thus, measured signal increases may result from a combination of concentration and environment changes. For this reason we suggest the use of the term 'apparent sodium concentration' (ASC) when the true quantitative nature of the sequence is in doubt. Note that, while this article has focused on potential signal loss related to residual quadrupole interactions, very rapid T_2 relaxation may also be a large (and potentially dominant) contributor to reduced ^{23}Na visibility in both healthy and diseased tissue.

As a result of this work, we suggest that the use of small flip-angles and very short RF pulses (large ω_1) will improve the accuracy of quantitative sodium concentration human brain imaging by reducing image contrast unrelated to sodium concentration (i.e. residual quadrupole related signal loss). For high field systems such as 7 T and 9.4 T, this may mean very high power pulses. Although prescribing flip-angles as small as 20° results in small absolute signal values, the facilitation of T_R reduction (while minimizing T_1 weighting) helps mitigate SNR inefficiency (i.e., more averaging is possible in a given scan time). Alternatively, exploration of novel pulse shaping may prove valuable (31). While residual quadrupole interactions may complicate quantitative sodium concentration imaging, they may also offer a new contrast mechanism to explore tissue structure and order. Recent sequences have been developed in this regard (32–34). It is possible that quantitative $\overline{\omega}_Q$ sodium MRI may offer new insight into the integrity of white matter in the brain.

Acknowledgements

Research sponsors were Alberta Innovates Health Solutions (CB – salary) and Natural Sciences and Engineering Research Council (operating).

REFERENCES

1. Inglese M, Madelin G, Oesingmann N, Babb JS, Wu W, Stoeckel B, Herbert J, Johnson G. Brain tissue sodium concentration in multiple sclerosis: a sodium imaging study at 3 tesla. Brain 2010; 133: 847–857.
2. Paling D, Solanky B, Riemer F, Tozer D, Wheeler-Kingshott C, Kapoor R, Golay X, Miller D. Sodium accumulation is associated with disability and progression in multiple sclerosis: a 23Na MRI study. J. Neurol. Neurosurg. Psychiatry 2013; 84(11): 2305–2317.
3. Zaaraoui W, Konstandin S, Audoin B, Nagel AM, Rico A, Malikova I, Soulier E, Viout P, Confort-Gouny S, Cozzone PJ, Pelletier J, Schad LR, Ranjeva JP. Distribution of brain sodium accumulation correlates with disability in multiple sclerosis: a cross-sectional Na-23 MR imaging study. Radiology 2012; 264(3): 859–867.
4. Mellon EA, Pilkinton DT, Clark CM, Elliott MA, Witschey WR, Borthakur A, Reddy R. Sodium MR imaging detection of mild alzheimer disease: preliminary study. Am. J. Neuroradiol. 2009; 30(5): 978–984.
5. Reetz K, Romanzetti S, Dogan I, Sass C, Werner CJ, Schiefer J, Schulz JB, Shah NJ. Increased brain tissue sodium concentration in huntington's disease – a sodium imaging study at 4 T. NeuroImage 2012; 63(1): 517–524.
6. Ouwerkerk R, Bleich KB, Gillen JS, Pomper MG, Bottomley PA. Tissue sodium concentration in human brain tumors as measured with Na-23 MR imaging. Radiology 2003; 227(2): 529–537.
7. Bartha R, Megyesi JF, Watling CJ. Low-grade glioma: correlation of short echo time H-1-MR spectroscopy with Na-23 MR imaging. Am. J. Neuroradiol. 2008; 29(3): 464–470.
8. Hussain MS, Stobbe RW, Bhagat YA, Emery D, Butcher KS, Manawadu D, Rizvi N, Maheshwari P, Scozzafava J, Shuaib A, Beaulieu C. Sodium imaging intensity increases with time after human ischemic stroke. Ann. Neurol. 2009; 66(1): 55–62.
9. Thulborn KR, Gindin TS, Davis D, Erb P. Comprehensive MR imaging protocol for stroke management: tissue sodium concentration as a measure of tissue viability in nonhuman primate studies and in clinical studies. Radiology 1999; 213(1): 156–166.
10. Bartha R, Menon RS. Long component time constant of Na-23 T^*_2 relaxation in healthy human brain. Magn. Reson. Med. 2004; 52(2): 407–410.
11. Rooney WD, Springer CS. A comprehensive approach to the analysis and interpretation of the resonances of spins 3/2 from living systems. NMR Biomed. 1991; 4(5): 209–226.
12. Berendsen HJC, Edzes HT. Observation and general interpretation of sodium magnetic resonance in biological material. Ann. N. Y. Acad. Sci. 1973; 204 30 Mar.: 459–485.
13. Halle B. Theory of intramolecular spin relaxation by translational diffusion in locally ordered fluids. 1. Continuum diffusion versus discrete-state exchange in systems with planar interfaces. Mol. Phys. 1984; 53(6): 1427–1461.
14. Reddy R, Bolinger L, Shinnar M, Noyszewski E, Leigh JS. Detection of residual quadrupolar interaction in human skeletal muscle and brain in vivo via multiple quantum filtered sodium NMR spectra. Magn. Reson. Med. 1995; 33(1): 134–139.
15. Tsang A, Stobbe RW, Beaulieu C. In vivo double quantum filtered sodium magnetic resonance imaging of human brain. Magn. Reson. Med. 2015; 73(2): 497–504.
16. Pandey L, Towta S, Hughes DG. NMR pulse response and measurement of the quadrupole coupling constant of $I = 3/2$ nuclei. J. Chem. Phys. 1986; 85(12): 6923–6927.
17. Joseph PM, Summers RM. The flip-angle effect – a method for detection of Na-23 quadrupole splitting in tissue. Magn. Reson. Med. 1987; 4(1): 67–77.
18. Abragam A. *Principles of Nuclear Magnetism*. Oxford University Press: New York, 1961.
19. Stobbe R, Beaulieu C. Advantage of sampling density weighted apodization over postacquisition filtering apodization for sodium MRI of the human brain. Magn. Reson. Med. 2008; 60(4): 981–986.
20. Dowell NG, Tofts PS. Fast, accurate, and precise mapping of the RF field in vivo using the 180° signal null. Magn. Reson. Med. 2007; 58(3): 622–630.

21. Sacolick LI, Wiesinger F, Hancu I, Vogel MW. B_1 mapping by Bloch–Siegert shift. Magn. Reson. Med. 2010; 63(5): 1315–1322.
22. Springer CS. *Biological Systems: Spin-3/2 Nuclei*. eMagRes, John Wiley & Sons, Ltd; 2007.
23. Stobbe RW, Beaulieu C. Assessment of averaging spatially correlated noise for 3-D radial imaging. IEEE Trans. Med. Imaging 2011; 30(7): 1381–1390.
24. Hancu I, van der Maarel JR, Boada FE. A model for the dynamics of spins 3/2 in biological media: signal loss during radiofrequency excitation in triple-quantum-filtered sodium MRI. J. Magn. Reson. 2000; 147(2): 179–191.
25. Woessner DE, Bansal N. Temporal characteristics of NMR signals from spin 3/2 nuclei of incompletely disordered systems. J. Magn. Reson. 1998; 133(1): 21–35.
26. Tsang A, Stobbe RW, Beaulieu C. Evaluation of B_0-inhomogeneity correction for triple-quantum-filtered sodium MRI of the human brain at 4.7 T. J. Magn. Reson. 2013; 230: 134–144.
27. Romanzetti S, Mirkes CC, Fiege DP, Celik A, Felder J, Shah NJ. Mapping tissue sodium concentration in the human brain: a comparison of MR sequences at 9.4 Tesla. NeuroImage 2014; 96: 44–53.
28. Romanzetti S, Halse M, Kaffanke J, Zilles K, Balcom BJ, Shah NJ. A comparison of three SPRITE techniques for the quantitative 3D imaging of the ^{23}Na spin density on a 4 T whole-body machine. J. Magn. Reson. 2006; 179(1): 64–72.
29. Shporer M, Civan MM. Nuclear magnetic resonance of sodium-23 linoleate-water. Basis for an alternative interpretation of sodium-23 spectra within cells. Biophys. J. 1972; 12(1): 114–122.
30. Choy J, Ling W, Jerschow A. Selective detection of ordered sodium signals via the central transition. J. Magn. Reson. 2006; 180(1): 105–109.
31. Lee JS, Regatte RR, Jerschow A. Optimal excitation of Na-23 nuclear spins in the presence of residual quadrupolar coupling and quadrupolar relaxation. J. Chem. Phys. 2009; 131(17): 174501.
32. Stobbe RW, Beaulieu C. Exploring and enhancing relaxation-based sodium MRI contrast. Magn. Reson. Mater. Phys. Biol. Med. 2014; 27(1): 21–33.
33. Laustsen C, Ringgaard S, Pedersen M, Nielsen NC. Quadrupolar-coupling-specific binomial pulse sequences for *in vivo* Na-23 NMR and MRI. J. Magn. Reson. 2010; 206(1): 139–146.
34. Lee JS, Regatte RR, Jerschow A. Selective detection of ordered sodium signals by a jump-and-return pulse sequence. J. Magn. Reson. 2009; 200(1): 126–129.